DOI: 10.24352/UB.OVGU-2017-055 TECHNISCHE MECHANIK, 34, 2, (2014), 90 – 103
submitted: January 8, 2013

Comparison of Different FE-Approaches for Modelling of Short Fibre Composites

J. Wilmers, B. Lenhof

In this article, four different FEM based methods for modelling of unidirectional short fibre composites are evaluated. The four methods differ in how they assign material properties. Method 1 and 2 assign them to whole elements while method 3 and 4 assign them to quadrature points. All four methods have in common that they use a structured mesh that does not resolve the microstructural geometry. This approach is in contrast to traditional methods in which the microstructure is mapped by a geometry-bound mesh, an approach that leads to work-intensive meshing and very small elements and thus high computational costs. The overall aim of all four methods is to reduce the computational costs caused by traditional meshing. The methods are evaluated with respect to their convergence behaviour and the obtained homogenised material properties. It is worked out that two of the four methods are well suited for modelling of complex microstructures.

1 Introduction

In the past decades the importance of composites as versatile and cost-effective construction materials has steadily increased. This is mainly due to the outstanding specific properties that can be achieved by reinforcing for example polymers with fibres. For highly heterogeneous materials such as short fibre composites the determination of homogenised effective material properties is of particular importance. The production and experimental analysis of specimen, however, is time and cost expensive, so theoretical methods are demanded in material and product development.

The oldest approach to calculate the effective material properties is the rule of mixture by Voigt (1887) and Reuss (1929). This model offers an upper and lower bound for the material stiffness but only considers the properties of matrix and inclusion material and the volume fraction. Thus, it is not able to describe a complex microstructure. Based on Eshelby's equivalent inclusion (Eshelby, 1957) a number of analytical models have been derived that allow for consideration of more parameters, e. g., the inclusion's aspect ratio and interaction between different inclusions. Prominent examples of these models are the Mori-Tanaka approach (Mori and Tanaka, 1973) or the Tandon-Weng method (Tandon and Weng, 1984). These analytical models are widely used in industrial development and production. For a review of the most common methods, refer to, e. g., (Gross and Seelig, 2007), (Tucker and Liang, 1999) or (Klusemann and Svendsen, 2010).

The analytical micro-mechanical models are limited by certain geometry assumptions and are not suitable to fully describe the properties of complex microstructures. With increasing computational power in the 1970s, computational homogenisation became a topic of interest because it makes the investigation of materials with complex microstructures possible. Computational homogenisation schemes usually utilise representative volume elements (RVE). The concept of RVEs was introduced by Hill in 1963, cf. (Hill, 1963), and refers to a volume that is big enough to contain a large enough number of inclusions to be representative but is small enough that the macroscopic fields are nearly constant over its volume. These conditions allow to consider the RVE as a point of the macrostructure and thus determine homogenised properties that are valid for every point of the material. The size of a RVE depends on a number of factors including, e. g., the ratio of the material's properties and the desired statistical quality (Kanit et al., 2003).

Often, the finite element method (FEM) is used to compute the effective properties of the composites. For this approach, the calculated stress and strain fields are homogenised over the RVE volume.

Using the FEM requires a discretisation of the RVE. Traditionally a geometry-bound mesh is used in FEM. For short fibre composites, this approach leads to very fine meshes with a lot of elements and the meshing itself often

is time-consuming and labour-intensive. To reduce the discretisation effort, there have been two main strategies in the last years. The first approach is the so called *meshless methods* which are for example described in (Belytschko et al., 1996) and (Idelsohn et al., 2003). The second one is the use of a structured mesh, e. g. Cartesian grids, for discretisation. This allows for fully automatisation of the meshing processes. Cartesian grids are used, among others, in *fictitious domain methods* which embed the physical area in a fictitious domain with a geometry that is easier to mesh (Vos et al., 2008; Burman and Hansbo, 2010, 2012; Bertoluzza et al., 2011; Parvizian et al., 2007). In (Kanit et al., 2003) and (Zeng et al., 2004), Cartesian grids have been used to model heterogeneous structures by assigning the material properties of different phases to the Gauß points, thus adopting mixed elements like they are used in *fictitious domain methods*. Based on the same approach, (Löhnert, 2004) introduced geometrically adaptive meshing using hanging nodes for better modelling of complex geometries. In (Sukumar et al., 2001) a structured grid is applied, too, while the different phases of the microstructure are modelled using level set functions as introduced by (Osher and Sethian, 1988). A different approach was introduced by Biabanaki and Khoei in 2012 (Biabanaki and Khoei, 2012). Here, the volume is discretised with a Cartesian grid first and the elements are refined so that the arising edges approximate the phase boundaries. Application of voxel meshing leads to a structured grid as well, cf. e. g. (Ernst et al., 2010). With this method, the meshing of the complex microstructures of real composites can be automated by utilising the voxel data optained from image processing.

In this article, four methods in the framework of the FEM that use a Cartesian grid are compared to determine which approach is most suited for modelling of a short fibre composite and calculation of its effective properties. The structure of the paper is as follows: In Section 2, the theoretical foundations and used equations are presented. The selected methods are described in Section 3 and Section 4 presents the realised simulations and their results. In Section 5, a brief summary of the findings is given.

2 Theory

In the present article, the effective macroscopic material properties of unidirectional short fibre composites are determined with different FEM simulations at the microscopic level. The FEM simulations differ in the way the microstructure is *numerically* modelled. However, the underlying *physical* model is the same for all computations.

Here, macroscopic level means a level where the composite can be identified as one homogeneous continuum, and microscopic level denotes a level where this continuum can be distinguished into separate homogenous phases. There is a need for the split into a macroscopic and a microscopic level since the characteristic length of the components in industrial applications is many times larger than the characteristic length of a fibre inclusion and a full resolution model would exceed today's computational possibilities.

To bridge the gap between the micro- and the macroscopic level, representative volume elements (RVE) as defined by (Hill, 1963), cf. Section 1, and testing volume elements (TVE) are utilised here. TVE refers to a section of a macroscopic volume that may have the same characteristic length as a corresponding RVE but does not fulfill the requirements of representativeness, i. e. its properties can't be generalised for the whole microstructure.

Under the assumption of small strain kinematics in Cartesian coordinates, the strain tensor at the microscopic level is given by

$$\boldsymbol{\varepsilon} = \frac{1}{2}[\operatorname{grad} \boldsymbol{u} + \operatorname{grad}^T \boldsymbol{u}] \tag{1}$$

where $\boldsymbol{u}$ is the displacement, $\boldsymbol{\varepsilon}$ the strain tensor and grad denotes the gradient operator. Moreover, only the static case of the momentum balance equations is taken into account

$$\operatorname{div} \boldsymbol{\sigma} = 0\,. \tag{2}$$

Here, $\boldsymbol{\sigma}$ represents the Cauchy stress tensor and div the divergence operator.

The material response of the polymer matrix and the fibres at microscopic level is modelled as linear elastic and isotropic

$$\boldsymbol{\sigma} = \boldsymbol{C}_i^{\mathrm{micro}} : \boldsymbol{\varepsilon} \qquad i = \{\mathrm{p}, \mathrm{f}, \mathrm{m}\} \tag{3}$$

where $\boldsymbol{C}_i^{\mathrm{micro}}$ is the stiffness tensor of either the polymer matrix, $i = \mathrm{p}$, or the fibres, $i = \mathrm{f}$, or a mixture of both, $i = \mathrm{m}$, depending on the numerical method used.

Finally, the values obtained from the microlevel are homogenised over the volume V via

$$\boldsymbol{\sigma}^{\mathrm{macro}} = \langle \boldsymbol{\sigma}^{\mathrm{micro}} \rangle := \frac{1}{V} \int_V \boldsymbol{\sigma}^{\mathrm{micro}} \, \mathrm{d}V \tag{4}$$

$$\boldsymbol{\varepsilon}^{\mathrm{macro}} = \langle \boldsymbol{\varepsilon}^{\mathrm{micro}} \rangle := \frac{1}{V} \int_V \boldsymbol{\varepsilon}^{\mathrm{micro}} \, \mathrm{d}V \, . \tag{5}$$

At the macroscopic level, transversal isotropy is assumed. Formulating the constitutive equation $\boldsymbol{\sigma}^{\mathrm{macro}} = \boldsymbol{C}^{\mathrm{macro}} : \boldsymbol{\varepsilon}^{\mathrm{macro}}$ of a hyperelastic, transversally isotropic material with regards to a structural tensor $\boldsymbol{M}$, which describes the material symmetry, allows to determine the respective stiffness tensor from the homogenised values from the microscopic level. In detail, the homogenised values are used to calculate the five independent, global material constants α_i that assemble the transversally isotropic stiffness tensor as follows

$$\begin{aligned} \boldsymbol{C}^{\mathrm{macro}} &= \frac{\partial \boldsymbol{\sigma}^{\mathrm{macro}}}{\partial \boldsymbol{\varepsilon}^{\mathrm{macro}}} \\ &= \alpha_1 \boldsymbol{I} \otimes \boldsymbol{I} + \alpha_2 (\boldsymbol{M} \otimes \boldsymbol{I} + \boldsymbol{I} \otimes \boldsymbol{M}) \\ &\quad + \alpha_3 (\boldsymbol{I} \otimes \boldsymbol{I})^{\frac{23}{T}} + \alpha_4 \boldsymbol{M} \otimes \boldsymbol{M} \\ &\quad + \alpha_5 \left[(\boldsymbol{M} \otimes \boldsymbol{I})^{\frac{23}{T}} + (\boldsymbol{I} \otimes \boldsymbol{M})^{\frac{23}{T}} \right] , \end{aligned} \tag{6}$$

where the notation $(\bullet)^{\frac{23}{T}}$ denotes the transposition with respect to the 2nd and the 3rd index of a fourth order tensor and $\boldsymbol{M}$ is a structural tensor defined by the directional vector $\boldsymbol{v}$, i. e. $\boldsymbol{M} = \boldsymbol{v} \otimes \boldsymbol{v}$, and $\boldsymbol{v}$ denotes the normal of the isotropic plane (cf. Ottosen and Ristinmaa (2005)). The normal of the isotropic plane itself changes in simulations due to different fibre angles. To still be able to compare results, the different solutions for the implemented fibre angles are projected to a reference direction of transverse isotropy, given by $\overline{\boldsymbol{v}} = (0, 1, 0)$. The α_i values in Equation 6 are defined in a global coordinate system. The projection to the reference direction is a conversion into a local coordinate system and, hence, it is possible to compare elements of $\boldsymbol{C}^{\mathrm{macro}}$ for different fibre angles.

3 Numerical Methods

The four methods investigated in this article all use a Cartesian grid but differ in the way the microstructure is modelled. The first method assigns the material properties of either fibre or matrix to a whole element depending on the phase the element's center is located in. This element-wise modelling is similar to classic geometry-bound discretisation but evidently leads to a falsification of the modelled geometry and probably to convergence problems when the mesh is not well chosen with respect to the microstructural geometry.

To counteract this effect, method 2 assigns "grey shades" of the properties to a whole element. Here, the properties are linearly interpolated depending on the fibre volume fraction in the element, e. g.

$$\boldsymbol{C}^{\mathrm{micro}}_{\mathrm{m}} = \phi \, \boldsymbol{C}^{\mathrm{micro}}_{\mathrm{f}} + (1 - \phi) \, \boldsymbol{C}^{\mathrm{micro}}_{\mathrm{p}} \, , \tag{7}$$

where ϕ is the fibre volume fraction and the indices m, f and p denote mixture, fibre and polymer values, respectively. This approach has to the best of the authors' knowledge not been applied to calculate effective material properties of short fibre composites before.

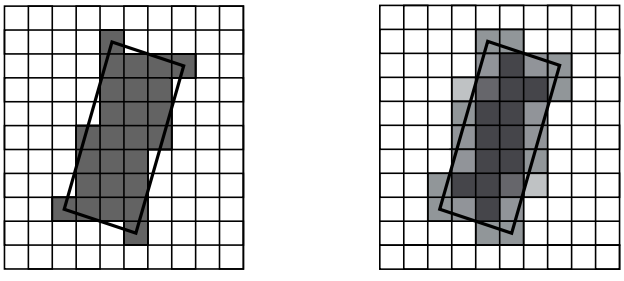

(a) (b)

Figure 1: Schematic illustration of the material property assignment in method 1 (a) and method 2 (b)

Both method 1 and method 2 use quadratic shape functions and an h-approach which here means that in every refinement step, the edge length of an element is cut in half.

In contrast to the first two methods, the other two methods assign the material properties independently of the element geometry. During assemblage of the system stiffness matrix, it is checked for every quadrature point whether it is located in the matrix or in a fibre. Depending on its location, the properties for either phase are used in assemblage, as schematically depicted in Figure 2.

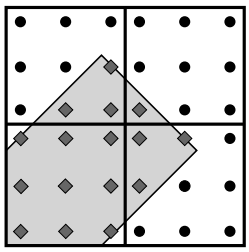

Figure 2: Schematic illustration of the material property assignment in methods 3 and 4.
Quadrature points that get fibre properties are depicted as diamonds.

The difference between methods 3 and 4 is that method 3 uses quadratic shape functions and increases the number of quadrature points to improve the modelling of the microstructure only, while method 4 uses a constant but high number of quadrature points and increases the function order. Method 4 is known as the *finite cell method* developed by Düster et al., a fictitious domain approach that uses high order functions to allow for better convergence (Parvizian et al., 2007; Schillinger et al., 2012; Düster et al., 2008; Düster and Rank, 2011; Düster et al., 2012). In fictitious domain methods, the numerical domain is larger than the physical domain. However, when simulating regularly shaped RVEs with the finite cell method, no fictitious material needs to be introduced, because the matrix serves as the embedding domain.

4 Simulations & Results

The numerical methods are programmed using the Open Source C++ program library deal.II (Bangerth et al., 2012, 2007). This allows for enhanced control of every program section and makes easy adjustments and extensions of the methods possible.

However, deal.II is not optimised for performance and the different methods make use of different parts of the library, so a reasonable discussion of computational time is not possible. To eliminate any influence of differing programme efficiency in the implementation, the required system sizes are compared, instead, to get an impression of computational costs.

In a first step, two-dimensional TVEs are simulated as a preliminary test to evaluate how well every method can model a microstructure. The simulated testing volumes are quadratic and contain only a single fibre. Their basic geometry is shown in Figure 3. The fibre is rotated relative to the structured mesh to analyse the modelling quality when the microstructure is oriented askew to the mesh's axes. For every method, the convergence behaviour, calculated effective properties and system size are observed to evaluate each method's quality and suitability.

In a second step based on these preliminary tests, only the promising methods are used to model three-dimensional

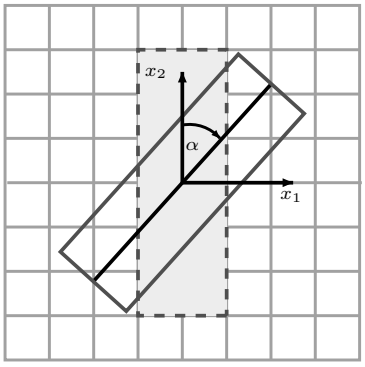

Figure 3: Geometry of the testing volume element

RVEs of a composite consisting of a PA 66 matrix and cylindrical glass fibres that are unidirectionally oriented. The composite is a transversely isotropic material and linear-elastic behaviour is assumed. The material constants are calculated with computational homogenisation and are compared with values determined for the same RVE with a geometry-bound mesh to show the quality of the calculated properties (Goldschmidt, 2011).

4.1 Testing Volume Elements

To investigate the convergence of all four methods the strain energy $U = \frac{1}{2} \int_V \boldsymbol{\sigma} : \boldsymbol{\varepsilon} \, \mathrm{d}V$ is taken into account.

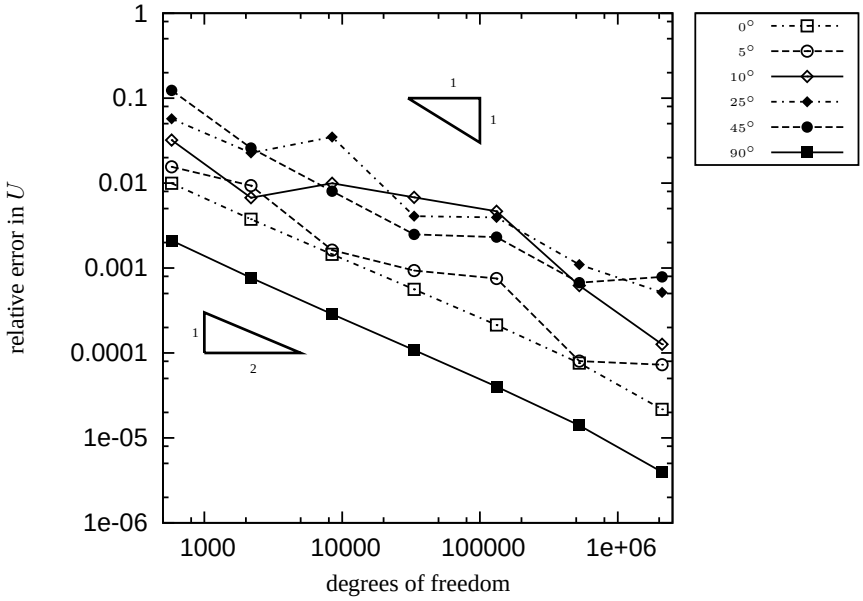

Figure 4: Convergence of method 1

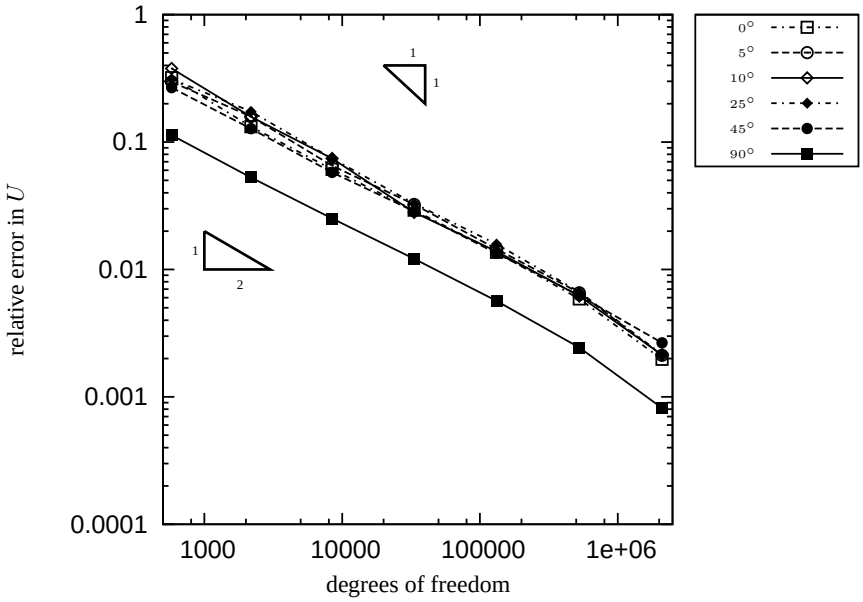

Figure 5: Convergence of method 2

In Figures 4, 5 and 8, the relative error in strain energy U for methods 1, 2 and 4 is plotted against the degrees of freedom. To get an impression of convergence rates there are triangles with different slopes depicted in the

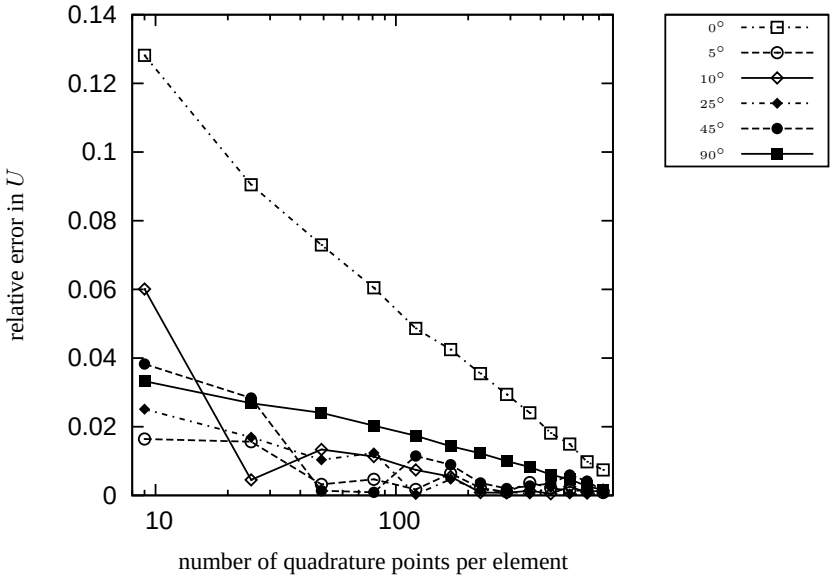

Figure 6: Convergence of method 3 for equidistant points

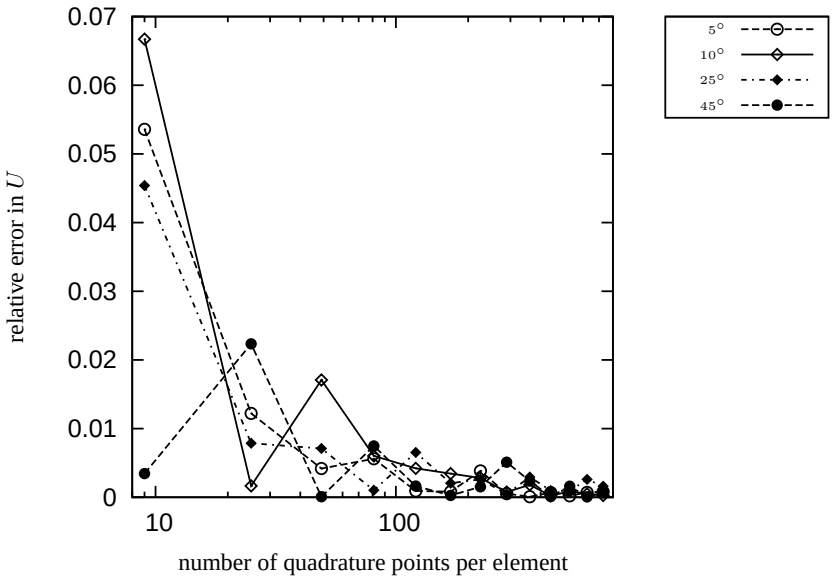

Figure 7: Convergence of method 3 for Gauß points

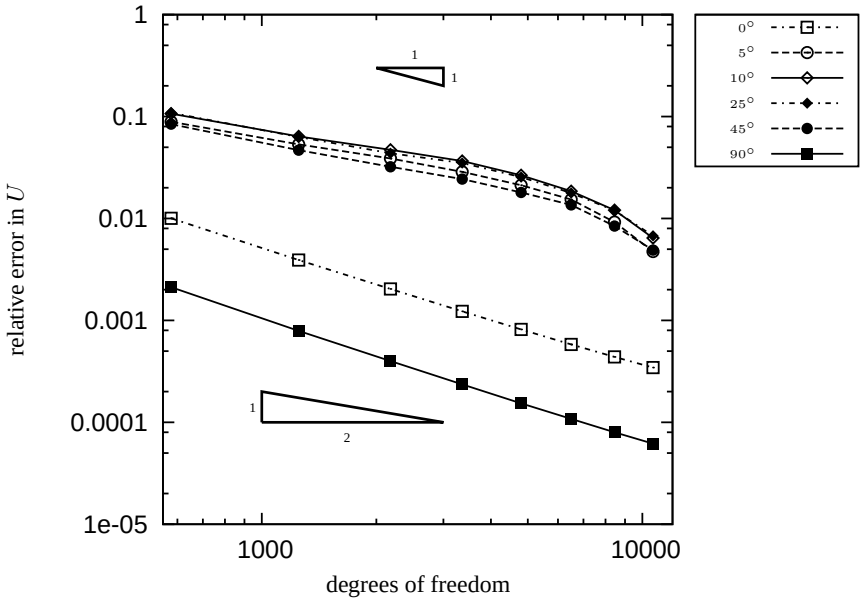

Figure 8: Convergence of method 4

figures. In Figure 5, the the relative error in U for method 3 is plotted against the number of quadrature points per element, because for this method, the number of degrees of freedom does not change. Due to lack of an analytical solution, the results a higher number of degrees of freedom or quadrature points, respectively, is used as reference to compute the relative error. The number that is deemed high enough for a reference is chosen as a compromise between calculation time and the visibility of the convergence behaviour.

In Figure 4, considerable fluctuations can be observed for angles different from $0°$ and $90°$. For these angles, the fibre is not aligned with the grid and edges appear in the modelled geometry. These edges seem to be responsible for the fluctuations in the results since the fluctuations vanish for $0°$ and $90°$.

Method 2 displays the anticipated smooth convergence behaviour as depicted in Figure 5. Here the measured relative errors are bigger than those observed for method 1, evincing that this method requires smaller elements and therefore very high numbers of degrees of freedom to approach almost constant values.

With method 3, calculations with both equidistant quadrature points (Newton-Cotes formulas) and Gauß quadrature have been carried out. Figure 6 indicates that a quadrature formula with changing intervals is favorable because of its steadier behaviour approaching an almost constant value at high quadrature point numbers. For $0°$ and $90°$, strain energies calculated with Gauß quadrature are independent of the number of quadrature points used. In contrast, calculations with Newton-Cotes formulas do not show any fluctuations when the fibres are aligned with the grid, but the calculated absolute values depend largely on the number of quadrature points per element. This behaviour is caused by stiffening of the adjacent elements by quadrature points on the element boundary. Hence, Gauß quadrature is superior to usage of equidistant quadrature points.

Method 4 offers a higher convergence rate compared to the other methods, especially for $0°$ and $90°$. For the other angles, the convergence rate increases for high function orders. This method exhibits different convergence behaviour for fibres that are aligned with the grid and those askew to it as opposed to method 2. But for both cases the convergence behaviour is smooth and this method has much smaller relative errors than method 2 at comparable system sizes.

Under the assumption of transverse isotropy, the effective material constants are calculated for every method. In Figure 9, the values of all four independent material constants and their dependence on the fibre angle are depicted. Here, x_2 is the fibre direction in a local coordinate system.

For different angles, the computed material values differ slightly. This variation appears for all four methods. It occurs because the testing volume elements are not representative of a certain microstructure. Rotating the fibre

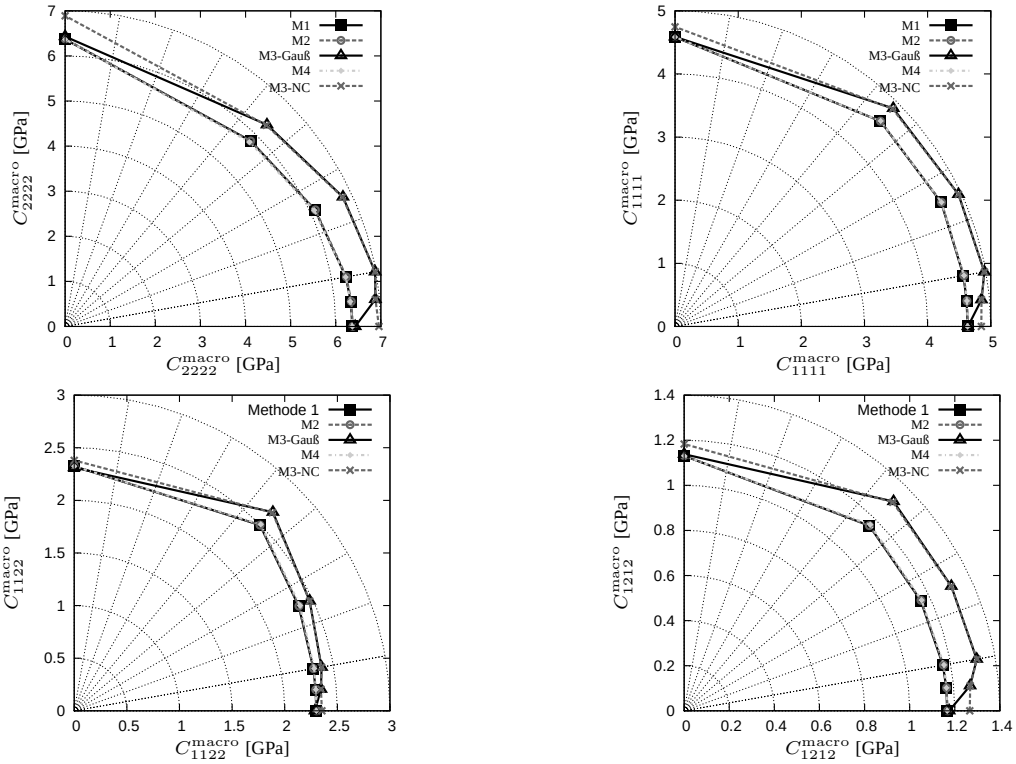

Figure 9: Angle dependency of the material constants $C^{\mathrm{macro}}_{ijkl}$ for different methods

changes the shortest distance between fibres and the pattern in the microstructure and thus causes the decrease in stiffness. This effect is observed for all methods, strengthening the hypothesis of a systematic modelling error. However, this error does not really affect the main object of study, i. e. the comparison of the different methods and thus is not addressed any further.

Methods 2 and 4 result in almost identical material constants. Despite the fluctuations while increasing the degrees of freedom, method 1 converges to the same result as methods 2 and 4. Method 3 overestimates the stiffness because the high number of quadrature points amplifies the stiffening effect displacement boundaries commonly have. This stiffening is due to the predetermination of a function form that has to be adhered by the shape functions. Extra quadrature points restricted the form of the shape functions even more, cf. (Liu and Quek, 2003). This effect is neglectible for the angles $0°$ and $90°$ when using Gaußpoints, because here no jumps in microstructural material stiffness occur within one element (and therefore, one shape function). Due to this behaviour, method 3 is not suitable to calculate effective material properties and is not considered in the following investigations.

For further comparison between the methods, the strain energy calculated with method 1 for 526,338 degrees of freedom is declared as a reference.

With method 1, a result differing less than 1 % from the reference can be achieved with a system of 8,450 degrees of freedom for $0°$. A fibre orientation of $45°$ impairs the quality, here 33,282 degrees of freedom are needed to lower the relative error beyond 1 %.
Method 2 requires even bigger system sizes. With this method, a system of 526,338 degrees of freedom gives a result that differs less than 1 % from the reference value for $0°$ as well as for $45°$. It is evident from this findings that method 2 in fact shows the anticipated indifference towards geometries that are not aligned with the grid, marking it an interesting approach for modelling of complex microstructures.
Like method 1, method 4 requires a bigger system to achieve the reference value for the unfavourably oriented fibre. The systems related to method 4, however, are a lot smaller than for the other two methods. To lower the error below 1 % 3,362 degrees of freedom are needed for $0°$ and 8,450 for $45°$.

Another important factor in the evaluation of the four methods is their ability to accurately depict the microstructural geometry. When traditional meshes are used, the microstructure is perfectly represented by the mesh. The use of a Cartesian grid, however, introduces changes in the modelled fibre volume depending on the way the material

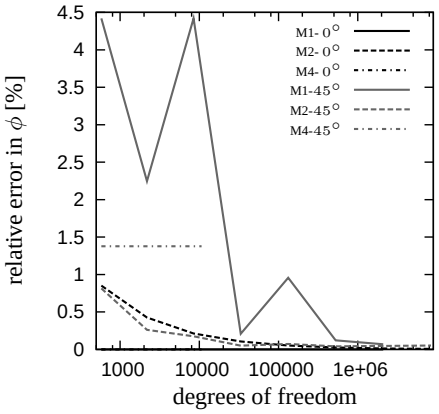

Figure 10: Change of modelled volume fraction over degrees of freedom

properties are assigned.

In Figure 10, the relative error of the modelled volume fraction ϕ to the geometrically predefined fibre volume fraction is depicted over the degrees of freedom. Method 2 displays a smooth convergence against the real value for both $0°$ and $45°$. In the latter case, small fluctuations are visible but the behaviour is smooth for both angles, as expected. Method 1, in contrast, models the real volume fraction independently of element size for fibres that are positioned favourably to the grid's axes. On the other hand, large fluctuations of the modelled volume appear for $45°$. As to method 4, the error does not change because element size and number of Gauß points are kept constant. Changing the number of Gauß points per element results in a change of the modelled fibre fraction, but this change is small and the modelled fraction is always about 1 % smaller than the real value. The same effect is observed for equidistant quadrature points. By increasing the number of quadrature points, no enhancement of the geometry modelling is possible. A way to achieve this is reducing the element size.

In summary, it can be said that with methods 1, 2 and 4 very similar effective material properties can be computed. To obtain these results, method 4 requires the smallest systems and thus is most effective concerning system size as an indicator of computational cost. Method 2 needs much bigger systems and higher run times. However, method 2 displays no differences in behaviour whether the fibre is oriented along the grid's axes or askew to them and thus is a very promising approach for simulation of complex microstructures with randomly oriented inclusions. Method 1 displays large fluctuations of the modelled volume fraction. However these fluctuations only result in small changes in strain energy and effective properties.

To investigate how well the calculated material constants concur with ones obtained with a geometry-bound meshing, comparative simulations of RVEs are carried out.

4.2 Representative Volume Elements

The three-dimensional representative volume elements are constructed using an algorithm developed by Goldschmidt (Goldschmidt, 2011). It places fibres into a predefined volume by generating random numbers for coordinates and checking for overlaps. Fibres that are intersected by the element's faces are continued on the opposite face, so that a periodic structure is achieved. The fibres are oriented along the x_3-axis. An example of the modelled microstructure is shown in Figure 11.

In (Goldschmidt, 2011), this algorithm is used to construct RVEs. The effective properties of it are calculated with a grid that follows the microstructural geometry. These results are considered as reference values hereafter to analyse whether the proposed methods are suitable alternatives to conventional meshing.

For our RVEs, the material properties of matrix and fibre are chosen according to Goldschmidt (2011), see Table 1.

Three instances of an RVE with a mass fraction of 20 % and differing fibre arrangement are simulated. A convergence analysis is carried out for the RVEs, too. The results are qualitatively the same as for the TVEs. For method 1, a distinct change in behaviour is visible for about 200,000 degrees of freedom which coincides with elements smaller than the fibre diameter so that for the first time all fibres are modelled. The convergence behaviour of

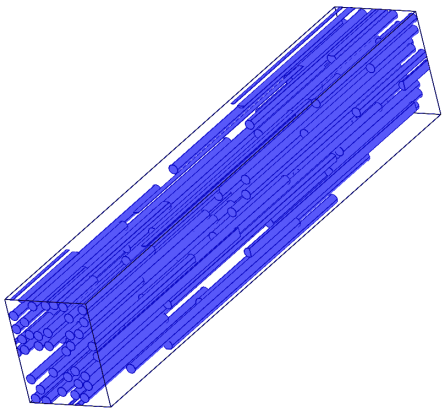

Figure 11: Example of the microstructure of the RVEs, with a volume fraction of 40 % (Goldschmidt (2011))

	Young's modulus	Poisson's ratio	mass densitiy
fibre	73 GPa	0.22	2.50 g/m^3
matrix	2,698 GPa	0.35	1.14 g/m^3

Table 1: Material properties used for the RVEs

methods 2 and 4 is smooth as seen before for the TVEs, although the errors in method 2 are about a magnitude bigger than for the other two methods. According to the results of this study, for methods 1 and 2 systems with ca. 12 million degrees of freedom are chosen. For method 4, a function order of 8 and 10^3 integration points per element are used, as a compromise between fast convergence due to a high number of integration points. This unfortunately leads to an overestimation of the material stiffness as described in the previous section and visible in Figure 12.

In Figure 12, the mean value and standard deviation of three different simulations of the RVE with a mass fraction of 20 % are depicted in comparison to the reference value. The grey lines indicate the mean value and the standard deviation of the reference results that are achieved with conventional meshing.

Method 1 displays a very small deviation and its mean value is almost identical to the reference. In contrast, methods 2 and 4 amount in higher material constants. The errors in convergence are large for method 2, so a possible explanation for the overestimation is that the considered system is too small. However, due to enormous run times, it was impossible to verify this theory.

While the described inadequacies in the applications of methods 2 and 4 have influence on the accuracy of the calculated material properties, they are insufficient to fully explain the artificial stiffening encountered for both methods. For method 2, the material properties of one finite element are interpolated with respect to the fibre volume fraction within the element. This corresponds to the application of the rule of mixture, i. e. the Voigt bound. A similiar approach is applied in method 4, where the material properties of either fibre or matrix are assigned to the Gauß points of the element. The values are interpolated linearly during quadrature, thus giving a Voigt-type result, cf. (Löhnert, 2004). It is well known, that the rule of mixture as applied in the Voigt approach overestimates the stiffness of a composite.

For both methods considered here, the difference is relatively small with 4.4 % and 4.0 % respectively. These errors are believed to be small enough as to be negligible for most technical applications.

For different mass fractions, further simulations are carried out. The results are depicted in Figure 13. This comparison shows that the good agreement between the proposed methods and the reference values is insensitive to the value of the mass fraction.

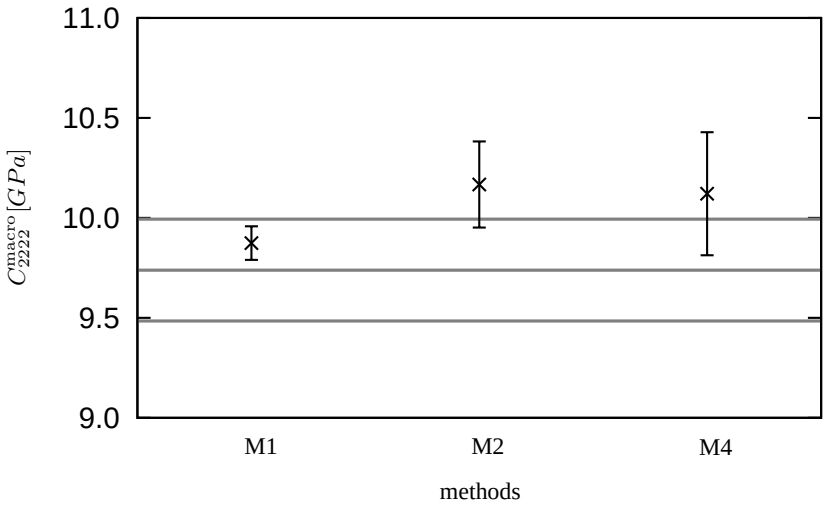

Figure 12: Comparison of the effective material properties obtained with the three methods and with conventional meshing

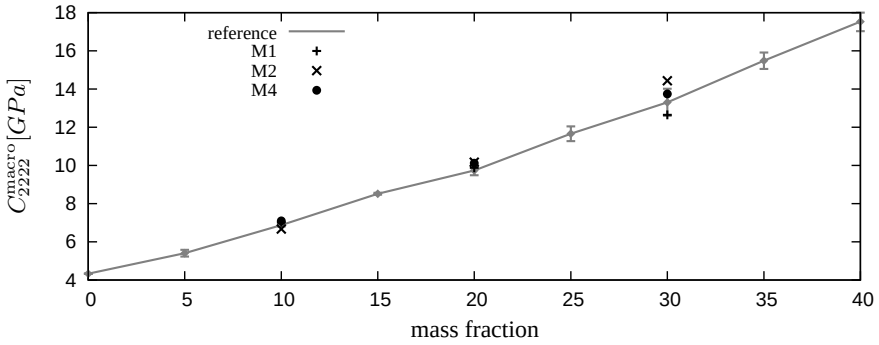

Figure 13: Comparison for different mass fractions

5 Conclusions

The simulations of testing volume elements show that three of the four proposed FEM based methods are suitable for modelling of short fibre composites and calculation of their effective properties, namely method 1, method 2 and method 4. Method 3 is unsuited for the given task, because the increasing number of integration points leads to artificial stiffening of the material. The use of equidistant points shows no advantage over Gauß points. With these three methods, effective material properties can be calculated that are in good agreement with results obtained by geometry-bound meshing. Method 1 assigns fibre and matrix properties to individual elements and gives the best results for RVEs with unidirectional fibres, but shows fluctuations for fibre orientations askew to the grid's axes. These fluctuations could prove to be problematic. Furthermore, the size of the needed finite elements is very small which leads to large system sizes and high computational times. Method 2 uses interpolated material properties for every element and displays the same characteristic but very smooth convergence. Both methods could highly benefit from implementation of adaptive refinement. Method 4, the *finite cell method*, assignes the material properties to quadrature points independently of the element geometry. Here, the simulated systems are much smaller. This method shows good convergence with increasing function order and the agreement with the reference solution obtained by geometry-bound meshing is good enough for the purposes of technical application.

Especially method 2 and method 4 are promising alternatives to conventional, geometry-bound meshing. In further investigations, it is of importance to optimise the software with respect to computational time and thus increase the efficiency. Following an optimisation like that, extensions of the physics that allow for studies of more realistic materials are aimed-at. Possible extensions are more complex material models that, e. g., take the matrix's viscoelastic behaviour into account or the implementation of failure mechanisms like delamination and fraction of the fibres.

Acknowledgements

This project has been financially supported by the *Stiftung Industrieforschung* with a scholarship. This support is gratefully acknowledged.

References

Bangerth, W.; Hartmann, R.; Kanschat, G.: deal.II – a general purpose object oriented finite element library. *ACM Trans. Math. Softw.*, 33, 4, (2007), 24/1–24/27.

Bangerth, W.; Heister, T.; Kanschat, G.: `deal.II` *Differential Equations Analysis Library, Technical Reference* (2012).

Belytschko, T.; Krongauz, Y.; Organ, D.; Fleming, M.; Krysl, P.: Meshless methods: An overview and recent developments. *Computer Methods in Applied Mechanics and Engineering*, 139, 1-4, (1996), 3–47.

Bertoluzza, S.; Ismail, M.; Maury, B.: Analysis of the fully discrete fat boundary method. *Numerische Mathematik*, 118, (2011), 49–77.

Biabanaki, S.; Khoei, A.: A polygonal finite element method for modeling arbitrary interfaces in large deformation problems. *Computational Mechanics*, 50, (2012), 19–33.

Burman, E.; Hansbo, P.: Fictitious domain finite element methods using cut elements: I. a stabilized Lagrange multiplier method. *Computer Methods in Applied Mechanics and Engineering*, 199, 41-44, (2010), 2680–2686.

Burman, E.; Hansbo, P.: Fictitious domain finite element methods using cut elements: II. a stabilized Nitsche method. *Applied Numerical Mathematics*, 62, 4, (2012), 328–341.

Düster, A.; Parvizian, J.; Yang, Z.; Rank, E.: The finite cell method for three-dimensional problems of solid mechanics. *Computer Methods in Applied Mechanics and Engineering*, 197, (2008), 3768–3782.

Düster, A.; Rank, E.: Die Finite Cell Methode - eine Fictious Domain Methode mit Finite-Element Ansätzen hoher Ordnung. *GAMM Rundbrief*, 2, (2011), 6–13.

Düster, A.; Sehlhorst, H.-G.; Rank, E.: Numerical homogenization of heterogeneous and cellular materials utilizing the finite cell method. *Computational Mechanics*, 50, 4, (2012), 413–431.

Ernst, G.; Vogler, M.; Hühne, C.; Rolfes, R.: Multiscale progressive failure analysis of textile composites. *Composite Science and Technology*, 70, (2010), 61–72.

Eshelby, J.: The determination of the elastic field of an ellipsoidal inclusion, and related problems. *Proceedings of the Royal Society of London*, A, 241, (1957), 376–396.

Goldschmidt, F.: *Effektive Eigenschaften von Faserverbünden in Abhängigkeit der Mikrotopologie*. Diplomarbeit, Universität des Saarlandes (2011).

Gross, D.; Seelig, T.: *Bruchmechanik - mit einer Einführung in die Mikromechanik*. Springer, Berlin/Heidelberg (2007).

Hill, R.: Elastic properties of reinforced solids: some theoretical principles. *Journal of the Mechanics and Physics of Solids*, 11, (1963), 357–372.

Idelsohn, S. R.; Oñate, E.; Calvo, N.; Pin, F. D.: The meshless finite element method. *International Journal for Numerical Methods in Engineering*, 58, 6, (2003), 893–912.

Kanit, T.; Forest, S.; Galliet, I.; Mounoury, V.; Jeulin, D.: Determination of the size of the representative volume element for random composites: statistical and numerical approach. *International Journal of Solids and Structures*, 40, (2003), 3647–3679.

Klusemann, B.; Svendsen, B.: Homogenization methods for multi-phase elastic composites: Comparsions and benchmarks. *Technische Mechanik*, 30, (2010), 374–386.

Liu, G.-R.; Quek, S.: *The Finite Element Method*. Butterworth-Heinemann, Oxford (2003).

Löhnert, S.: *Computational Homogenization of Microheterogeneous Materials at Finite Strains Including Damage*. Phd-thesis, Universitt Hannover (2004).

Mori, T.; Tanaka, K.: Average stress in matrix and average elastic energy of materials with misfitting inclusions. *Acta Metallurgica*, 21, 5, (1973), 571–574.

Osher, M.; Sethian, J.: Fronts propagating with curvature-dependent speed: algorithms based on Hamilton-Jacobi formulations. *Journal of Computational Physics*, pages 12–49.

Ottosen, N.; Ristinmaa, M.: *The Mechanics of Constitutive Modelling*. Elsevier, Oxford (2005).

Parvizian, J.; Düster, A.; Rank, E.: Finite cell method. *Computational Mechanics*, 41, (2007), 121–133.

Schillinger, D.; Düster, A.; E.Rank: The hp-d-adaptive finite cell method for geometrically nonlinear problems of solid mechanics. *International Journal for Numerical Methods in Engineering*, 89, (2012), 1171–1202.

Sukumar, N.; Chopp, D.; Moes, N.; Belytschko, T.: Modeling of holes and inclusions by levelsets in the extended finite-element method. *Computer Methods in Applied Mechanics and Engineering*, 190, 48, (2001), 6183–6200.

Tandon, G.; Weng, G.: The effect of aspect ratio of inclusions on the elastic properties of unidirectionally aligned composites. *Polymer Composites*, 5, 4, (1984), 327–333.

Tucker, C. L.; Liang, E.: Stiffness predictions for unidirectional short-fiber composites: Review and evaluation. *Composites Science and Technology*, pages 59–655.

Vos, P.; van Loon, R.; Sherwin, S.: A comparison of fictitious domain methods appropriate for spectral/hp element discretisations. *Computer Methods in Applied Mechanics and Engineering*, 197, (2008), 2275–2289.

Zeng, T.; Wu, L.-Z.; Guo, L.-C.: Mechanical analysis of 3d braided composites: a finite element model. *Composite Structures*, 64, 3-4, (2004), 399–404.

Addresses:
M.Sc. Jana Wilmers
Institute of Materials Research, Materials Mechanics
Helmholtz-Zentrum Geesthacht
Max-Planck-Str. 1
21502 Geesthacht, Germany
jana.wilmers@hzg.de

Dr.-Ing. Bernd Lenhof
Lehrstuhl für Technische Mechanik
Universität des Saarlandes
Campus A4 2, Zi. 1.07
66123 Saarbrücken, Germany
b.lenhof@mx.uni-saarland.de